The Leucotriene C_4 Binding Sites in Multidrug Resistance Protein 1 (ABCC1) Include the First Membrane Multiple Spanning Domain†

Joel Karwatsky,‡ Mara Leimanis,‡ Jie Cai,§ Philippe Gros,§ and Elias Georges*,‡

Institute of Parasitology and Department of Biochemistry, McGill University, Ste-Anne-de-Bellevue, Quebec H9X 3V9, Canada

Received June 3, 2004; Revised Manuscript Received October 13, 2004

ABSTRACT: The *m*ultiple drug *r*esistance *p*rotein 1 (MRP1 or ABCC1) transports anticancer drugs and normal cell metabolites. Leucotriene C_4 (LTC_4) is one of the highest affinity substrates of MRP1. In this study, we have synthesized and characterized a novel photoreactive azido analogue of LTC_4 ($AALTC_4$). The specificity of $AALTC_4$ binding to MRP1 was confirmed using an LTC_4-specific monoclonal antibody. Moreover, binding with radioiodinated [^{125}I]$AALTC_4$ (or $IAALTC_4$) to MRP1 was dramatically competed with unmodified LTC_4 and to a lesser degree by glutathione (GSH). Oxidized glutathione (GSSG) slightly increased $IAALTC_4$ binding to MRP1, while MK571, verapamil, and vincristine inhibited $IAALTC_4$ binding to MRP1. Using $AALTC_4$ together with a panel of epitope-specific and LTC_4-specific monoclonal antibodies, we identified LTC_4 binding sites in MRP1. Western blotting of large tryptic fragments of MRP1 with three well-characterized epitope-specific mAbs (MRPr1, QCRL1, and MRPm6) showed LTC_4 binding in both the N- and C-terminal halves of MRP1. Furthermore, a peptide corresponding to the N-terminal membrane-spanning domain of MRP1 (MSD0) was photoaffinity labeled by $AALTC_4$, indicating that MSD0 contains an LTC_4 binding site. Higher resolution mapping of additional LTC_4 binding sites was obtained using eight MRP1 variants with each containing hemaglutanin A (HA) epitopes at different sites (at amino acid 4, 163, 271, 574, 653, 938, 1001, or 1222). MRP1 variants were photoaffinity labeled with $IAALTC_4$ and digested with trypsin to isolate specific regions of MRP1 that interact with LTC_4. These results confirmed that sequences in MSD0 interact with $IAALTC_4$. Other regions that were photoaffinity labeled by $IAALTC_4$ include TM 10−11, TM 16−17, and TM 12, shown previously to encode MRP1 drug binding site(s). Together, our results show a high-resolution map of LTC_4 binding domains in MRP1 and provide the first direct evidence for LTC_4 binding within MSD0.

Chemotherapy is commonly used in the treatment of malignant tumors in cancer patients. Unfortunately, treatment of patients with anticancer drugs often fails due to the rise of chemoresistant tumors. Using in vitro tumor model systems, several proteins have been identified to cause resistance to multiple anticancer drugs. P-glycoprotein (P-gp1 or ABCB1) was the first protein identified and shown to efflux anticancer drugs (*1*). This transmembrane protein was shown to bind and transport a diverse group of compounds, thereby conferring multidrug resistance (MDR)[1] (*2*, *3*). A decade after its discovery, several MDR cell lines were identified that did not overexpress P-gp1 (*4*, *5*). These cells expressed another membrane protein termed the multidrug resistance-associated protein (MRP1 or ABCC1) (*6*). Both P-gp1 and MRP1 function as broad-specificity drug pumps that bind and transport drugs against a concentration gradient using ATP hydrolysis (*7*, *8*). P-gp1 and MRP1 confer resistance to natural product drugs including epipodophyllotoxins, vinca alkaloids, and certain anthracyclines (*9*−*11*). Unlike P-gp1, the substrates of MRP1 include a range of amphiphilic organic anions. Many of its substrates are conjugated with glutathione (GSH), glucuronate, or sulfate (*12*). Moreover, several of the conjugated and nonconjugated compounds such as aflatoxin B_1 and vincristine display a dependence on GSH for their transport (*13*, *14*). The clinically relevant nonconjugated antimetabolite, methotrexate, is also directly transported by MRP1 (*10*). The transport of substrates via MRP1 has been largely determined by their ability to inhibit the transport of LTC_4, one of the highest affinity MRP1 substrates (*13*). LTC_4, along with other cysteinyl leukotrienes, is a mediator of immediate hypersensitivity reactions, acting as a potent agonist of bronchoconstriction and vascular permeability (*15*, *16*). Studies with *mrp1*$^{-/-}$ mice have shown LTC_4 to be an important natural substrate of MRP1 due to their impaired LTC_4-mediated inflammatory response (*17*). Another study showed that dendritic cell mobilization and trafficking into lymphatic vessels are reduced in *mrp1*$^{-/-}$ mice; this effect was restored

† This work was supported by the Natural Sciences and Engineering Research Council (NSERC) and the Canadian Institute of Health Resrarch (CIHR) (to E.G.), as well as by the National Cancer Institute of Canada (to P.G.).

* To whom correspondence should be addressed. Tel: 514 398 8137. Fax: 514 398 7857. E-mail: Elias.Georges@McGill.CA.

‡ Institute of Parasitology, McGill University.

§ Department of Biochemistry, McGill University.

[1] Abbreviations: ABC, ATP-binding cassette; GSH, glutathione; GSSG, oxidized glutathione; HA, hemagglutinin A; $IAALTC_4$, [^{125}I]-iodoarylazidoleucotriene C_4; LTC_4, leucotriene C_4; mAb, monoclonal antibody; MDR, multidrug resistance; MRP1, multidrug resistance protein 1; P-gp1, P-glycoprotein 1; SDS−PAGE, sodium dodecyl sulfate−polyacrylamide gel electrophoresis.

10.1021/bi048853h CCC: $30.25
Published on Web 12/04/2004

by exogenously adding LTC_4 (*18*). These studies have proved a valuable in situ tool to confirm that LTC_4 is a natural substrate of MRP1.

MRP1 has 17 predicted transmembrane (TM) helices and two nucleotide binding domains (NBD) that hydrolyze ATP (*19*−*21*). The TM regions are divided into three core membrane multiple spanning domains (MSD). The first (MSD0) encodes five TM helices, while the two others (MSD1 and MSD2) contain six TM helices each. Although a region equivalent to MSD0 does not exist in P-gp1, the organization of MSD1 and MSD2 is similar to the topology of P-gp1. The third cytoplasmic loop (CL3) in MRP1 connects MSD0 to the P-gp1-like core of MSD1 and MSD2 and is termed linker domain 0 (L0). Two protease hypersensitive sites exist in MRP1, one in L0 and the other in the NBD1/MSD2 linker (L1). These sites can generate protein fragments capable of associating to form a functional transporter. The predicted topological organization of MRP1 from the NH_2 terminus to the COOH terminus of the protein proceeds as follows: MSD0-*L0*-MSD1-NBD1-*L1*-MSD2-NBD2 (*20*, *21*). Recently, we have examined the substrate binding sites in MRP1 using radiolabeled photoreactive substrates of MRP1. The compounds have widely differing structures and interact with MRP1 in functionally diverse ways. These include two quinoline analogues (IAAQ and IACI), a modified analogue of the fluorescent rhodamine 123 (IAARh123), and an analogue of glutathione (IAAGSH). Interestingly, each of these compounds reacts with TM 10−11 and TM 16−17 in MSD1 and MSD2, respectively (*22*, *23*). Subsequent amino acid replacement studies have also identified these regions as potential substrate binding sites (*24*−*28*), in addition to other domains in MRP1 which appear to affect primarily drug transport or MRP1-mediated MDR (*29*−*32*). Indeed, studies using [^{3}H]LTC_4 have been shown to photoaffinity label MRP1 (*13*, *33*−*36*); however, the low labeling efficiency has limited its use. In this study, we synthesized a radiolabeled photoreactive analogue of LTC_4 ([^{125}I]iodoarylazidoleucotriene C_4 or $IAALTC_4$) in an effort to obtain a high-resolution map of its binding domains in MRP1. Our findings revealed that $IAALTC_4$ interacts specifically with MRP1 at physiologically relevant binding sites. The location of LTC_4 binding occurred within TM 10−11 and TM 16−17, in addition to TM 12 of MRP1. Interestingly, we found that $IAALTC_4$ interacted with and photolabeled the MSD0 domain of MRP1.

EXPERIMENTAL PROCEDURES

Materials. Protein A−Sepharose CL-4B and carrier-free sodium [^{125}I]iodide (100 mCi/mL) were purchased from Amersham Pharmacia Biotech (Baie d'Urfe, Quebec, Canada). ImmunoPure immobilized protein G, trypsin (sequencing grade and TPKC treated), and NHS-ASA were purchased from Pierce (Rockford, IL). Leukotriene C_4 (LTC_4) was purchased from Biomol (Cedarlane Laboratories, Ltd., Hornby, Ontario, Canada). The monoclonal anti-hemagglutinin A monoclonal antibody (mAb) 16B12 (anti-HA) was purchased from Berkeley Antibody Co. (Richmond, CA). Leukotriene C4/D4/E4 Ab-1 mAb was obtained from Neo-Markers (Medicorp, Quebec, Canada). Anti-MRP1, clone MRPm6, MRPr1, and QCRL1 mAbs were acquired from Kamiya Biomedical Co. (Seattle, WA). Protease inhibitor cocktail for mammalian tissues was purchased from Sigma (St. Louis, MO). All other chemicals were of the highest possible quality.

Cell Culture and Plasma Membrane Preparation. HeLa cells were cultured in α-MEM media containing 10% fetal bovine serum (Hyclone). HeLa cells transfected with MRP1-HA variants had a stable expression of MRP1 containing one or more copies of the hemagglutinin A (HA) epitope (YPYDVPDYAS) inserted after amino acid 1, 163, 271, 574, 653, 938, 1001, or 1222 from the N-terminus (*37*, *38*). For plasma membrane preparations, cells were detached with trypsin−EDTA and washed with phosphate-buffered saline, pH 7.4 (PBS). The cell pellet was then resuspended in hypotonic buffer (1 mM $MgCl_2$, 10 mM KCl, 10 mM Tris-HCl, pH 7.4) containing protease inhibitors. Cells were lysed in a Dounce homogenizer and centrifuged at 10000*g* for 5 min followed by a second centrifugation at 100000*g* for 1 h. The final pellet was resuspended in buffer M (5 mM Tris-HCl, 250 mM sucrose, pH 7.4) and stored at −70 °C. Protein concentrations were determined by the Lowry method (*39*).

Synthesis of $AALTC_4$. The synthesis of a photoreactive analogue of LTC_4, arylazido-LTC_4 ($AALTC_4$), was done as previously described (*40*) with some modifications. All manipulation was preformed in dark-room conditions. Briefly, 200 μg of LTC_4 (dissolved in methanol/ammonium acetate buffer, 65:35, pH 5.6) was dried. The full amount was dissolved in 200 μL of dimethylformamide (DMF), followed by the addition of 0.02% (v/v) triethylamine. Finally, NHS-ASA (dissolved in DMF) was added to produce a final reaction containing 0.8 mM LTC_4, 3.2 mM NHS-ASA, and 0.01% triethylamine in 400 μL, pH 8−9. The reactants were allowed to incubate for 48 h at room temperature with rotation. The reaction was terminated, and the resulting mixture was separated on high-performance liquid chromatography using a reverse-phase C18 column from Grace Vydac (Hesperia, CA). Separation was achieved using a 90 min gradient of 0−100% acetonitrile in 0.025 M ammonium acetate buffer, pH 5.5. Purified $AALTC_4$ was characterized by mass spectrometry, then dried, and stored at −70 °C.

Iodination of $AALTC_4$. $AALTC_4$ was dissolved in 10 μL of methanol/ammonium acetate buffer, 65:35, pH 5.6, and mixed with 100 μL of 3 μg/μL chloramine T prepared in sodium phosphate buffer (10 mM, pH 8.5) along with 5 mCi of carrier-free Na^{125}I (100 mCi/mL). The reaction proceeded for 5 min at room temperature and was stopped with 100 μL of 5% sodium metabisulfite in sodium phosphate buffer. The sample was then loaded on a C18 SepPak column that was preequilibrated with 100% methanol, followed by methanol/sodium phosphate buffer (10:90). After injection of the reaction into the column, it was washed 10−20 times with 5 mL aliquots of methanol/sodium phosphate buffer (10:90) to remove free iodine. $IAALTC_4$ was eluted from the column with 5 mL of 100% methanol and then dried. The iodinated sample was resuspended in 100−200 μL of methanol/ammonium acetate buffer, 65:35, pH 5.6.

Plasma Membrane Vesicle Preparation. Plasma membranes were prepared as follows. Cells were centrifuged for 45 min at 100000*g* at 4 °C. The pellet was resuspended in a hypotonic lysis buffer containing 10 mM KCl, 1.5 mM $MgCl_2 \cdot 6H_2O$, 10 mM Tris-HCl, pH 7.4, and protease inhibitors. The cells were homogenized with 20 strokes using a tight-fitting Dounce homogenizer and centrifuged for 10 min at 10000*g* at 4 °C. The supernatant was removed and

set aside while the pellet was resuspended in TS buffer (50 M Tris-HCl, 250 mM sucrose, pH 7.4) and homogenized with another 20 strokes; the suspension was centrifuged for 10 min at 10000*g* at 4 °C. The supernatant was combined with the supernatant from the first centrifugation and centrifuged for 45 min at 100000*g* at 4 °C. The pellet was resuspended in TS buffer. For vesicle preparation, the final pellet was passed through a 27-gauge needle 30 times. The protein concentration was determined using the Lowry method (*39*). The plasma membranes and vesicles were snap-frozen in liquid nitrogen and stored at −70 °C.

Photoaffinity Labeling and SDS−PAGE. For photoaffinity labeling, IAALTC$_4$ (0.1−1 μM) was added to 20−40 μL aliquots of plasma membrane (20−100 μg) in TS buffer and incubated at room temperature for 30 min, in the dark. Samples were further incubated on ice for 10 min followed by UV irradiation at 254 nm for 10 min, as previously described (*40*). Photolabeled samples underwent proteolytic digestion and immunoprecipitation (*41*), as described below. Protein samples were resolved on SDS−PAGE exclusively using the Fairbanks system (*42*). Coomassie Blue staining was used to detect all proteins in plasma membrane samples. Alternatively, gels with radiolabeled proteins were dried and exposed on Kodak BIOMAX MS film at −70 °C.

Proteolytic Digestion and Immunoprecipitation. Photoaffinity-labeled plasma membrane samples (100 μg) were digested with increasing concentrations of trypsin at 37 °C for 40 min. The digestion was stopped by placing the samples on ice and adding 80 μL of IP buffer A (1% SDS, 50 mM Tris-HCl, pH 7.4) with protease inhibitors. Samples were left on ice for 15 min before the addition of 320 μL of IP buffer B (1.25% Triton X-100, 190 mM NaCl, 0.05 M Tris-HCl, pH 7.4). The digested peptides were immunoprecipitated as previously described (*41*). Briefly, samples were incubated overnight with protein A−Sepharose beads conjugated to anti-HA mAb. After incubation, samples were washed five times with IP buffer C (0.05% Triton X-100, 0.03% SDS, 150 mM NaCl, 5 mg/mL BSA, 0.05 M Tris-HCl, pH 7.4) and once with IP buffer D (150 M NaCl, 0.05 M Tris-HCl, pH 7.4). For immunoprecipitation with the MRPr1 mAb, plasma membrane samples were precleared with 50 μL of ImmunoPure immobilized protein G for 30 min. The protein G beads were removed, and the samples were incubated overnight with 2 μg of the mAb. After incubation, 50 μL of ImmunoPure immobilized protein G was added to each sample and incubated for 30 min at room temperature and 2 h at 4 °C. The samples were then washed five times with IP buffer C and once with IP buffer D and resolved by SDS−PAGE.

N-Glycosidase F (PNGase F) Digestion of MRP1 and Polypeptides. Deglycosylation of MRP1 or proteolytic fragments was performed as previously described (*43*). Briefly, after the immunoprecipitation washes, purified MRP1 was denatured by adding 10 μL of 0.1 M 2-ME/0.1% SDS to the immobilized protein A or G pellets and heating for 5 min at 65 °C. The denatured MRP1 was transferred to a fresh tube, and the following components were added in order: 3 μL of 0.5 M Tris-HCl (pH 8.6), 5 μL of H_2O, 2 μL of 10% Triton X-100, and 5 μL of 1 unit/mL PNGase F. The samples were then incubated overnight at 37 °C in the presence of protease inhibitors and resolved by SDS−PAGE.

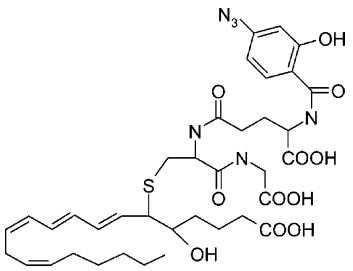

FIGURE 1: Chemical structure of arylazidoleucotriene C$_4$ (AALTC$_4$).

Western Blotting. For immunodetection of MRP1, 20 μg of enriched plasma membranes was resolved on SDS−PAGE and transferred to nitrocellulose membrane by using a wet electroblotting technique as outlined in Towbin et al. (*44*). The nitrocellulose membrane was blocked in PBS with 5% skim milk and incubated with MRPr1, QCRL1, MRPm6, and anti-LTC$_4$ mAbs for 2 h at room temperature. After incubation, membranes were washed and incubated for 2 h with 1:3000 (v/v) goat anti-mouse or anti-rat antibodies conjugated to horseradish peroxidase. SuperSignal West Pico or Femto chemoluminescent substrate (Pierce, Rockford, IL) was used to detect mAb binding.

Vesicle Transport of IAALTC$_4$ and [^{3}H]LTC$_4$. Transport of IAALTC$_4$ and [^{3}H]LTC$_4$ into membrane vesicles was determined by rapid filtration as described, with modifications (*13*). The membrane vesicles were diluted in TS buffer and passed through a 27-gauge needle five times. Transport assays were carried out at 23 °C in a buffer containing 1 mM ATP, 10 mM $MgCl_2$, 10 mM phosphocreatine, 0.1 unit/μL creatine kinase, and 50 nM [^{3}H]LTC$_4$ or IAALTC$_4$, in TS buffer. At specific time intervals, aliquots were removed and added to 1 mL of ice-cold TS buffer. Each sample was then filtered through 0.22 μm nitrocellulose filters on a vacuum manifold. The filters were washed three times with 3 mL of cold TS buffer and solubilized before quantifying the radioactivity. All data were corrected for the amount of [^{3}H]LTC$_4$ or IAALTC$_4$ that bound nonspecifically to the filters in the absence of membrane vesicles.

RESULTS

In an effort to isolate LTC$_4$ substrate binding sites in MRP1, we synthesized a photoreactive analogue of LTC$_4$, arylazido-LTC$_4$ (AALTC$_4$) (Figure 1), and characterized its modification by mass spectrometry. Figure 2A shows AALTC$_4$ photoaffinity-labeled plasma membranes from HeLa and MRP1-transfected HeLa cells immunoprecipitated with an MRP1-specific mAb (MRP1r1) and then probed with an LTC$_4$-specific mAb (lanes 1 and 2, respectively). The specificity of the photoreactive analogue (AALTC$_4$) toward MRP1 is illustrated by the observation that the LTC$_4$-specific mAb reacted with a 190 kDa protein in plasma membranes from MRP1-transfected but not HeLa plasma membranes. The results of this Western blot also confirm the integrity of the photoreactive analogue (AALTC$_4$) as it is recognized by an anti-LTC$_4$ mAb which binds native LTC$_4$. Indeed, previous efforts to identify LTC$_4$ binding domains using [^{3}H]-LTC$_4$ have been of limited success largely due to the low efficiency of photolabeling of MRP1 with LTC$_4$ and the time required to obtain a reasonably detectable signal. Thus, AALTC$_4$ was further iodinated (IAALTC$_4$) and used to photoaffinity label plasma membranes prepared from HeLa

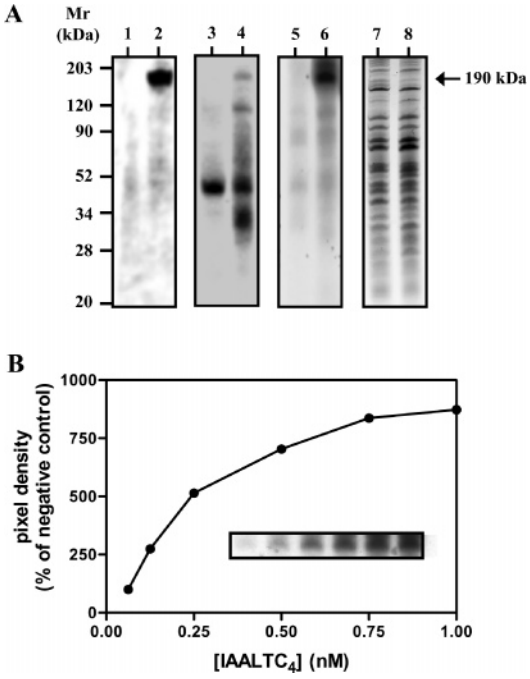

FIGURE 2: Photolabeling of HeLa and HeLa-MRP1 with $AALTC_4$ and $IAALTC_4$. Western blot analysis using an anti-LTC_4 mAb was used to detect $AALTC_4$ photolabeling in HeLa and HeLa-MRP1 membrane proteins (lanes 1 and 2, respectively). Lanes 3 and 4 show photolabeled HeLa and HeLa-MRP1 membrane proteins with MRP1-specific mAb (MRPr1). Lanes 5 and 6 show an immunoprecipitation of $IAALTC_4$-photolabeled HeLa and HeLa-MRP1 membrane proteins with MRP1-specific mAb (MRPr1). Lanes 7 and 8 show the staining of membrane proteins from HeLa and HeLa-MRP1 with Coomassie Blue. The graph in panel B demonstrates the saturable photoaffinity labeling of MRP1 with increasing amounts of $IAALTC_4$.

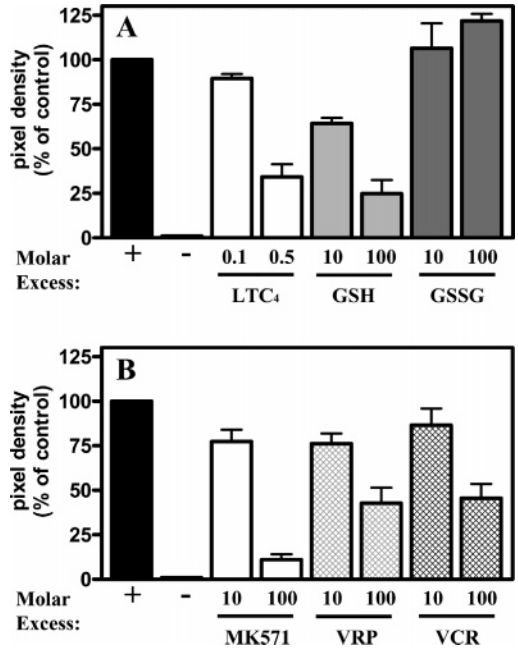

FIGURE 3: Effect of several drugs on photolabeling of MRP1 by $IAALTC_4$. Panel A shows the change in photolabeling of MRP1 with $IAALTC_4$ in the absence or presence of several endogenous compounds: LTC_4, reduced glutathione (GSH), and oxidized glutathione (GSSG). Panel B shows photolabeling with $IAALTC_4$ in the absence or presence of exogenous drugs: MK571, verapamil (VRP), and vincristine (VCR). LTC_4 was added at a 0.1 and 0.5 molar concentration excess of $IAALTC_4$. All other drugs were added in 10 and 100 molar concentration excess of $IAALTC_4$. Plasma membranes were immunoprecipitated with hemagglutinin A (HA) mAb. The intensity of photolabeling is expressed relative to MRP1 photolabeled with $IAALTC_4$ alone and measured using the Bio-Rad Quantity One program. All samples were photolabeled and immunoprecipitated with an MRP1-specific mAb. Each condition was repeated at least three times in duplicate.

and MRP1-transfected HeLa cells (Figure 2A, lanes 3 and 4, respectively). Specific photolabeling of a ~190 kDa protein can be seen in MRP1-transfected but not in untransfected cells. Furthermore, the results in Figure 2A (lanes 5 and 6) show samples immunoprecipitated with the MRP1-specific mAb, MRPr1. A radiolabeled polypeptide with a molecular mass of ~190 kDa was found only in lane 6 of Figure 2A, demonstrating that $IAALTC_4$ specifically photoaffinity labeled MRP1. Membrane proteins from HeLa and MRP1-transfected HeLa cells were visualized with Coomassie Blue (Figure 2A, lanes 7 and 8, respectively). Since there was no detectable increase in expression of a 190 kDa protein, it can be inferred that specific photolabeling of MRP1 by $IAALTC_4$ is not exclusively caused by overexpression. The specificity of $IAALTC_4$ to MRP1 was further confirmed when increasing concentrations of $IAALTC_4$ were used to saturate the binding site(s). Figure 2B shows that the intensity of photoaffinity labeling of MRP1 levels off as the concentration of $IAALTC_4$ is increased from 0.0625 to 1 μM. This saturation of photolabeling indicates that the LTC_4 analogue interacted with a physiologically relevant site within MRP1 and is consistent with the high affinity of LTC_4 toward MRP1.

To determine whether $IAALTC_4$ interacts with the same binding sites as other MRP1 substrates, MRP1-enriched plasma membranes were photolabeled in the presence of various MRP1 substrates. Figure 3A shows the effect of increasing concentrations of three endogenous substrates on MRP1 labeling: LTC_4, GSH, and GSSG. The addition of very low concentrations of LTC_4 showed significant binding competition of $IAALTC_4$ to MRP1. In fact, a 0.1 molar excess (or 10% of the total $IAALTC_4$ concentration) produced a small, yet significant, reduction in photolabeling. Furthermore, at 0.5 molar excess (or 50%), LTC_4 reduced photolabeling by more than 60%. Interestingly, GSH produced a similar decrease as seen with LTC_4 although at a significantly higher molar concentration (100 μM). In contrast, 10 μM GSSG, also a substrate of MRP1 (*45*), had no effect, while 100 μM GSSG caused a slight increase in MRP1 photolabeling with $IAALTC_4$ (~25%).

It was also of interest to examine the photolabeling of MRP1 in the presence of several exogenous substrates of MRP1: MK571, verapamil, and vincristine (Figure 3B). Each of these compounds are transported or cotransported by MRP1 (*46*−*49*). All three drugs caused a moderate decrease in the intensity of MRP1 labeling at a molar concentration of 10 μM. At 100 μM, MK571 reduced the photolabeling of MRP1 by more than 80%. This observation is consistent with a previous finding that MK571 acts as a competitor in the photolabeling of MRP1 by [^{3}H]LTC_4 (*34*). Binding competition was less effective with both verapamil and vincristine at 100 μM, with each causing approximate 50% competition. This is consistent with the higher affinity of MRP1 for MK571 compared to verapamil or vincristine (*46*−*50*). These findings show that $IAALTC_4$ photolabels a

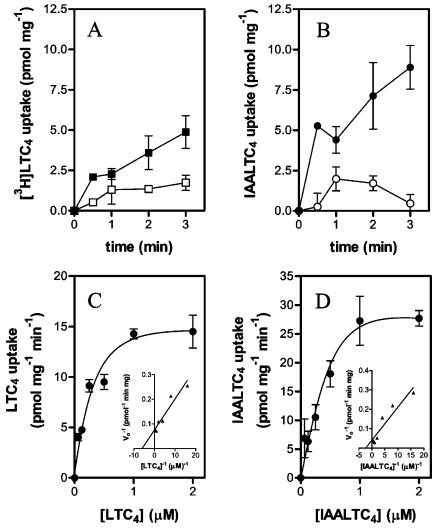

FIGURE 4: Uptake of [^{3}H]LTC_4 and $IAALTC_4$ by membrane vesicles from MRP1-transfected and control HeLa cells. The uptake of 50 nM [^{3}H]LTC_4 and $IAALTC_4$ into membrane vesicles is shown in panels A and B, respectively. The uptake of each compound was measured at several time points from 0 to 3 min. Open symbols represent uptake in vesicles derived from HeLa cells; closed symbols show uptake in vesicles from MRP1-transfected HeLa cells. Panels C and D show uptake of [^{3}H]LTC_4 and $IAALTC_4$, respectively, into vesicles from MRP1-transfected HeLa cells at various concentrations (0.0625−2 μM) for 2 min at 23 °C. The kinetic parameters, K_m and V_{max}, were determined from regression analysis of the Lineweaver−Burk transformation of the data (insets).

binding site that overlaps or interacts with known substrates of MRP1.

To determine if $IAALTC_4$ is transported by MRP1 in an ATP-dependent manner, its transport was measured using inside-out membrane vesicles prepared from HeLa and MRP1-transfected HeLa cells. Since transport of [^{3}H]LTC_4 into vesicles has been extensively studied, it was of interest to investigate $IAALTC_4$ transport and compare it to [^{3}H]-LTC_4. Figure 4A shows the time-dependent uptake of [^{3}H]-LTC_4 into vesicles. This graph shows a correlation between LTC_4 transport and levels of MRP1 expression, whereby vesicles from MRP1-transfected cells show higher uptake than the HeLa vesicles. The levels of [^{3}H]LTC_4 uptake did not exceed 6 pmol mg^{-1} after 3 min, which is relatively low compared to previous studies using vesicles isolated from H69/AR cells which have a very high level of MRP1 expression (*35*). A similar difference due to the level of MRP1 expression was seen in the uptake of $IAALTC_4$ although the maximum uptake at 3 min did not exceed 10 pmol mg^{-1} (Figure 4B). The lower uptake of [^{3}H]LTC_4 compared to $IAALTC_4$ indicated that [^{3}H]LTC_4 may have a lower transport rate than $IAALTC_4$. To resolve this, the rates of uptake for $IAALTC_4$ at several concentrations were measured to compare K_m and V_{max} for transport in membrane vesicles (Figure 4C). It is apparent that vesicular uptake becomes saturated above 1 μM $IAALTC_4$. The Lineweaver−Burk double reciprocal plot of a single experiment produced an apparent K_m of 0.42 μM and a V_{max} of 25.25 pmol mg^{-1} min^{-1} (inset of Figure 4C). The average K_m and V_{max} values for three experiments were 0.26 ± 0.17 μM and 24.00 ± 4.78 pmol mg^{-1} min^{-1}. As a comparison, we measured the same kinetic parameters with [^{3}H]LTC_4, obtaining a K_m of 0.17 ± 0.053 μM and a V_{max} of 13.7 ± 1.07 pmol mg^{-1} min^{-1} (Figure 4D).

The primary goal of this study was to identify the photolabeling sites of LTC_4 in MRP1. To do so, we made use of the well-established MRP1 trypsin digestion profile together with an anti-LTC_4-specific mAb to initially identify the large fragments of MRP1 that interacted with LTC_4. The identity of MRP1 trypsin digestion patterns was confirmed using MRP1 epitope-specific mAbs [e.g., the mAb MRPr1 epitope is between amino acids 238−247 (*51*), QCRL1 recognizes amino acids 918−924 (*52*), and MRPm6 recognizes amino acids 1511−1520 (*51*)]. The most visible product of digestion and immunoblotting with the MRPr1 mAb is a polypeptide of 120 kDa (Figure 5A). This fragment has previously been identified under similar conditions and corresponds to the NH_2-proximal half of MRP1 (*21*). The trypsin-sensitive site that generates this fragment is well documented and found within the L1 cytoplasmic loop (*52*). Although this fragment was detected in the absence of trypsin, its intensity was dramatically increased as the concentration of trypsin was increased. The 120 kDa polypeptide has previously been labeled as N1 (*21*). In addition to N1, a second polypeptide is visible with a broad molecular mass of 45−55 kDa; this fragment has been named N2 (*21*). N2 corresponds to a fragment that extends from the amino terminal to a digestion site within the L0 cytoplasmic linker region within CL3 (*20*). Two other antibodies, QCRL1 and MRPm6, react with regions on the COOH-proximal side of the L1 trypsin-sensitive site. QCRL1 reacts with an epitope in the L1 cytoplasmic loop of MRP1. Digestion and Western blotting with QCRL1 produced a 111 kDa fragment named C1. This fragment extends from the L1 trypsin-sensitive site to the carboxyl terminal of MRP1 (Figure 5B). In addition, two other polypeptides were generated at trypsin concentrations of 1:100 and 1:10 (trypsin:protein). The larger one, at approximately 42 kDa, we named C2. A smaller 29 kDa band, C3, is also visible at 1:100. Both C2 and C3 were not detected in a previous study using similar conditions (*21*); perhaps a greater amount of plasma membrane was used per sample in the current study. In fact, we could not detect either the C2 or C3 fragments with less than 25 μg of plasma membrane (data not shown). The MRPm6 antibody reacts with an epitope in the cytoplasmic loop on the COOH-proximal side of MSD2. It was also able to detect the C1 fragment with increasing trypsin concentrations (Figure 5C). In addition, MRPm6 detected a 35 kDa polypeptide at the highest trypsin concentration (1:10) (named C4). An illustration of the various MRP1 tryptic fragments and their positions relative to MRP1 topology is shown directly below Figure 5A−C. Using the tryptic profile of MRP1, we determined which peptides were photolabeled by noniodinated $AALTC_4$ using an LTC_4-specific mAb. Figure 5D shows MRP1-enriched membranes photolabeled and digested before immunoblotting with the LTC_4-specific mAb. The N1 fragment was the most clearly visible polypeptide in the Western blot. This band indicates that $AALTC_4$ photolabeled the NH_2-terminal portion of MRP1. Additional polypeptides were visible at the highest concentration of trypsin (1:10). These bands correspond to N2 and C2. This further localizes the binding of $AALTC_4$ to the regions encompassed by N2 and C2, namely, MSD0-L0 and MSD2, respectively. Although these bands are less distinct

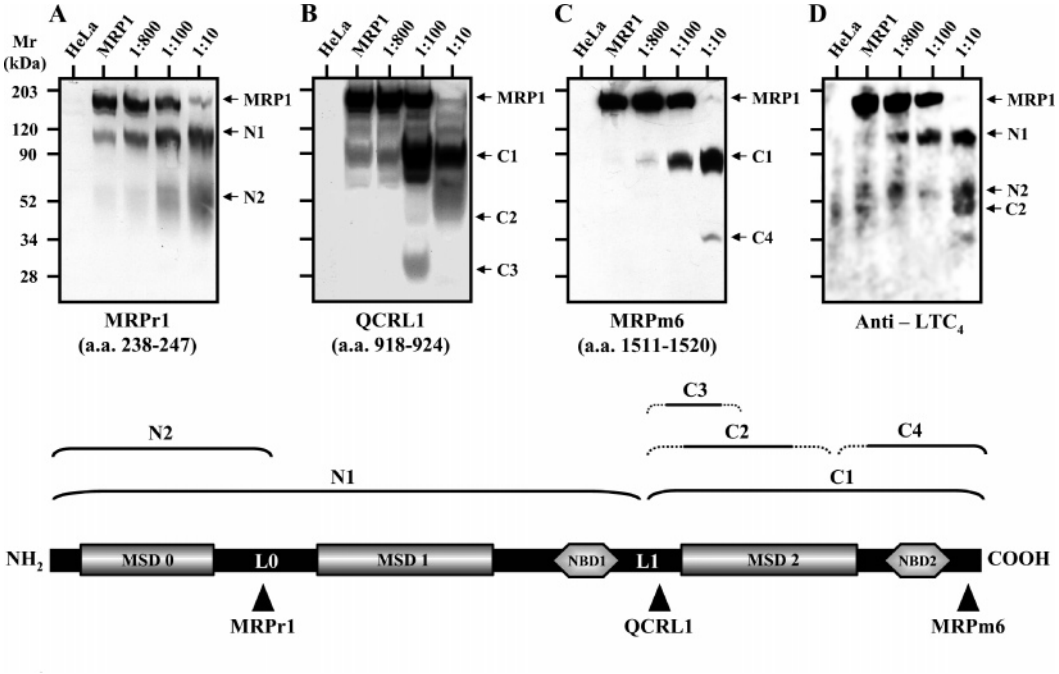

FIGURE 5: Western blot analyses of MRP1 peptides generated by limited trypsin proteolysis. MRP1 from transfected HeLa cells was digested with increasing concentrations of trypsin (trypsin:protein). The proteolytic fragments were detected by Western blot using three MRP1-specific monoclonal antibodies: MRPr1, QCRL1, and MRPm6 (panels A−C, respectively). MRP1 was also photolabeled with $AALTC_4$, digested, and probed with an anti-LTC_4 antibody (panel D). For clarification, the epitope for each antibody is indicated on a topological illustration of MRP1. The size and location of each peptide are also shown.

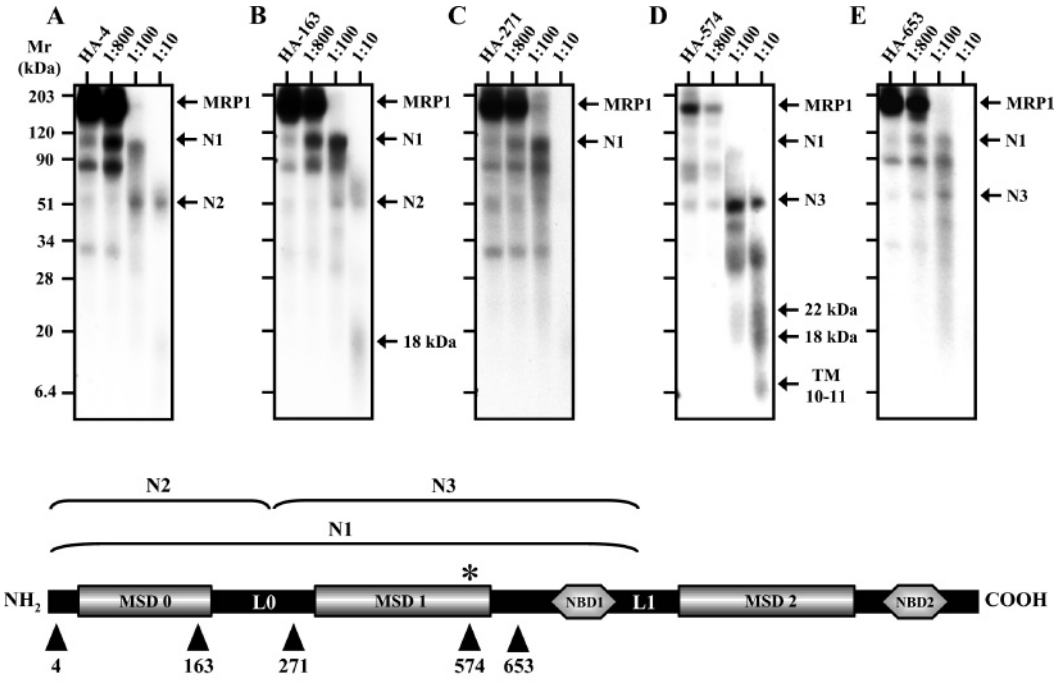

FIGURE 6: Photolabeling and digestion of N-terminal MRP1-HA variants. Five different MRP1-HA variants (4, 163, 271, 574, and 653) were photolabeled with $IAALTC_4$, digested with trypsin (trypsin:protein), and immunoprecipitated with an anti-HA antibody. The location of each HA epitope is indicated on a topological illustration of MRP1. The size and location of peptides are also shown; the asterisk indicates the location of a localized photolabeling site.

than those seen in Figure 5A−C, their resolution is impressive considering that very low amounts of $AALTC_4$ were used to photolabel MRP1.

We have previously localized the binding sites of several photoreactive drugs using MRP1 proteins with HA epitopes inserted at eight different sites, after amino acid 4, 163, 271, 574, 653, 938, 1001, or 1222 (*22*, *23*). Figures 6 and 7 show results obtained using these eight different MRP1-HA variants photolabeled with $IAALTC_4$ and digested with increasing concentrations of trypsin. Proteolytic fragments containing the HA epitope were immunoprecipitated with an HA-specific mAb, and $IAALTC_4$ photolabeled fragments were identified. Panels A and B of Figure 6 show two proteolytic peptides from MRP1 variants 4 and 163, whereby

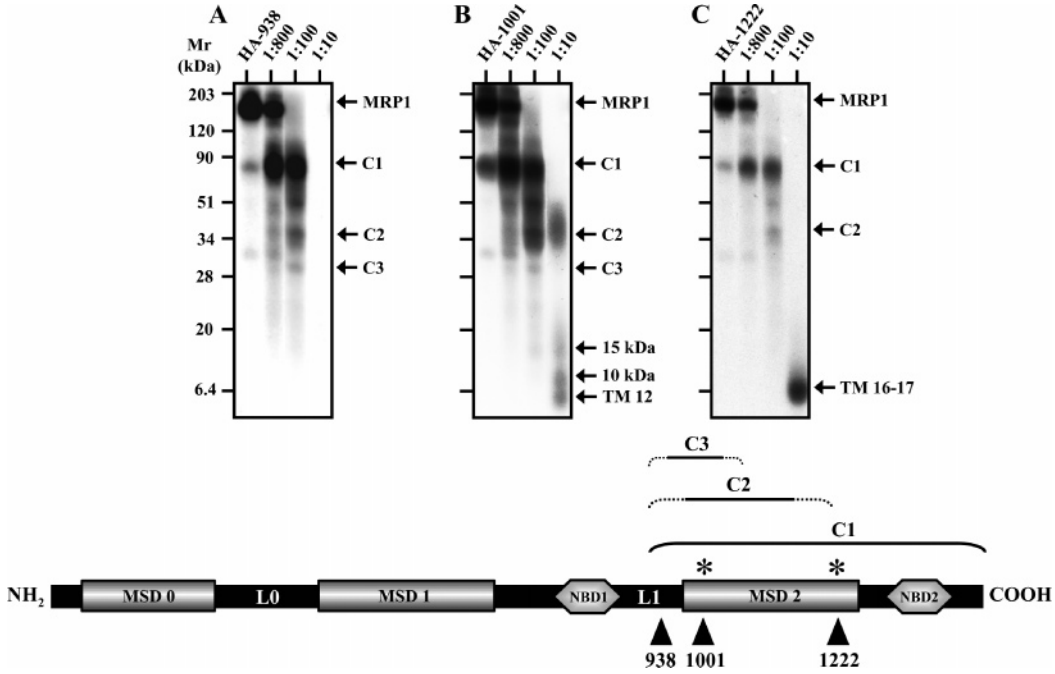

FIGURE 7: Photoaffinity labeling and digestion of C-terminal MRP1-HA variants. Three different MRP1-HA variants (938, 1001, and 1222) were photolabeled with $IAALTC_4$, digested with trypsin (trypsin:protein), and immunoprecipitated with an anti-HA antibody. The location of each HA epitope is indicated on a topological illustration of MRP1. The size and location of the peptides are also shown; the asterisks show localized photolabeling sites.

the largest fragment corresponds to the 111 kDa or N1 fragment identified in Figure 5A. The other polypeptide that was photolabeled by $IAALTC_4$ corresponds to the 50−60 kDa or N2 fragment, visible at higher concentrations of trypsin (1:100 and 1:10). The appearance of the N1 and N2 fragments indicates that a photolabeling site is found in the NH_2-proximal portion of MRP1 as well as in MSD0. In addition to the N1 and N2 fragments, an 18 kDa polypeptide is visible in MRP1 variant 163 (Figure 6B). This further localizes the photolabeling site to the COOH-proximal side of the N2 fragment. The N2 fragment was not visible in the MRP1 variant 271 because the trypsin site is located on the N-terminal side of this epitope. Only the N1 fragment was produced at trypsin concentrations of 1:800 and 1:100 with MRP1 variant 271 (Figure 6C). MRP1 variant 574 yielded a larger spectrum of photolabeled polypeptides in addition to the N1 fragment (Figure 6D). Digestion of this MRP1 variant at the highest trypsin concentration (1:10) generated three bands with the approximate sizes of 22, 18, and 6.5 kDa. The appearance of these bands correlates with fragments identified with other photoreactive drugs: IACI, IAARh123, and IAAGSH (*22*, *23*). Consequently, the sequence of the 6.5 kDa fragment has previously been determined as ^{542}SAYLSAVGTFTWVCTPFLVALCTFAVYVTIDEN-**[HA][HA]**NILDAQTAFVSLALFNILR^{593}. The underlined portion of the linear amino acid sequence corresponds to the proposed TM 10 and TM 11. The mass of this fragment is calculated to be 6.9 kDa, which is identical to the size of the peptide in Figure 6D. The position of the HA epitopes and the size of the smallest peptide limit the region of photolabeling to TM 10−11. A 52−55 kDa polypeptide was also visible in the digested MRP1 variant 574. This polypeptide corresponds to a previously identified fragment named N3 (*21*). The N3 fragment is a polypeptide bordered by the L0 and L1 trypsin-sensitive sites. We believe that $IAALTC_4$ photolabels the N3 fragment because the size of the polypeptide and the position of the HA epitope correlate with the characteristics of N3. The N3-like fragment was also clearly photolabeled with $IAALTC_4$ in MRP1 variant 653.

The results from MRP1 variants 938, 1001, and 1222 are shown in panels A, B, and C of Figure 7, respectively. An 85 kDa polypeptide is visible in the digestion pattern of all three MRP1 variants in Figure 7. This band corresponds to the C1 fragment that was characterized by Western blot (Figure 5B,C). C1 is generated at a trypsin concentration of 1:800 and 1:100 in these three MRP1 variants. This confirms that $IAALTC_4$ photolabeled the COOH-proximal "half" of MRP1. In addition, a 38 kDa fragment was photolabeled in MRP1 variants 938, 1001, and 1222. This corresponds to the mass of the smallest trypsin fragment that encompasses the MRP1 amino acid sequence between 938 and 1222 (including the mass of HA epitopes). The size of this band corresponds to the C2 fragment identified in Figure 5B. Moreover, the C3 fragment identified in Figure 5B was also photolabeled in MRP1 variants 938 and 1001 (Figure 7A,B). Interestingly, digestion of MRP1 variant 1001 produced three previously unidentified photolabeled polypeptides with molecular masses of 15, 10, and 6 kDa. The following sequence is the smallest tryptic fragment that contains the HA epitope at position 1001: ^{969}AIGLFISFLSIFLFMCNHVSALAS-NYWLSLWT**[HA][HA]**DDPIVNGTQEHTK^{1013}. The underlined portion represents the predicted TM 12. The calculated molecular mass of this polypeptide is 7.4 kDa. This is the first time a distinct photolabeling site has been identified in this region of MRP1. The results in Figure 7C show that $IAALTC_4$ photoaffinity labels a 7 kDa tryptic peptide in the digested MRP1 variant 1222. As with MRP1 variant 574, this peptide has been previously identified with several other photoreactive drugs (*22*, *23*). On the basis of the molecular mass of the photoaffinity-labeled peptide and

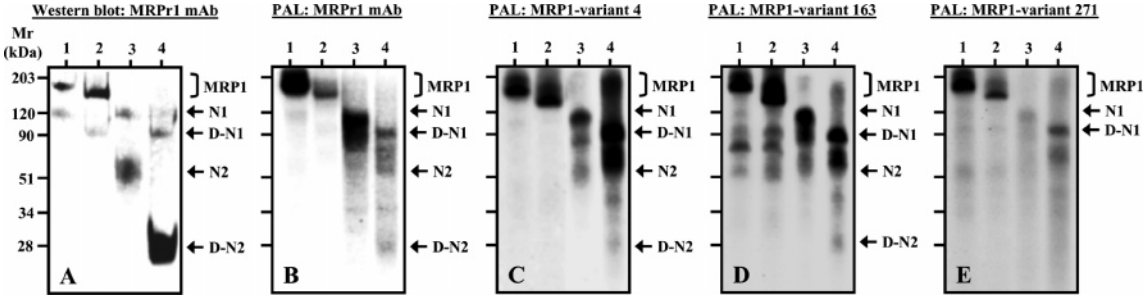

FIGURE 8: Deglycosylation of the photolabeled N2 peptide. In each panel, lane 1 contains MRP1-enriched plasma membrane, lane 2 has MRP1 deglycosylated with PNGase F, lane 3 shows MRP1 digested with trypsin (1:10 trypsin:protein), and lane 4 shows MRP1 digested and deglycosylated. MRPr1 antibody was used for the Western blot (panel A). Panels B−E show MRP1-HA variants (4, 163, and 271) that were photoaffinity labeled (PAL) with IAALTC$_4$ followed by immunoprecipitation with MRPr1 (panel B) or anti-HA antibodies (panels C−E).

the trypsin cleavage site in the vicinity of position 1222, photoaffinity labeling occurs within the following sequence: ^{203}LECVGNCIVLFAALFAVIS**[HA][HA]**RHSLSAGLVGLSVSYSLQVTTYLNWLVR^{1249}. The underlined regions represent the predicted location of TM 16 and TM 17. The calculated molecular mass of this peptide, including the HA epitopes, is 7 kDa. The illustrations located below Figures 6 and 7 show topological drawings of MRP1 with the relative position of each HA epitope and the polypeptides that are produced by trypsin digestion. The asterisks indicate the location of isolated IAALTC$_4$ photolabeling sites.

The photolabeling of the N2 polypeptide with IAALTC$_4$ in MRP1 variants 4 and 163 was particularly interesting. This is the first time that a photolabeling site has been demonstrated within MSD0. Using [^{3}H]LTC$_4$, a previous study examining LTC$_4$ binding sites in MRP1 concluded that MSD0 does not contain a photolabeling site (*36*). To further confirm the photoaffinity labeling of the N2 fragment with IAALTC$_4$, we made use of the glycosylation status of the N2 fragment. A previous study indicated that N2 could be deglycosylated to produce a 25 kDa fragment (*21*). To confirm the results of the latter study, MRP1 was incubated with and without PNGase F and digested with trypsin, and the resultant peptides were examined by Western blot using the MRPr1 mAb. The first lane of Figure 8A shows that the MRPr1 mAb reacts with MRP1 and the trypsin-derived N1 fragment from MRP1-enriched plasma membranes. The second lane of Figure 8A shows the same sample treated with PNGase F; the sizes of both MRP1 and N1 were decreased due to deglycosylation. With trypsin digestion, the 45−55 kDa N2 fragment was detected (Figure 8A, lane 3). After deglycosylation with PNGase F, N2 was reduced to 25−30 kDa (Figure 8A, lane 4). On the basis of these results, we surmised that the IAALTC$_4$-labeled N2 fragment would appear as a 25−30 kDa band after deglycosylation. To test this, MRP1 was photolabeled with IAALTC$_4$ and then digested with trypsin (1:10). The peptides were immunoprecipitated with the MRPr1 mAb followed by treatment with PNGase F. Lanes 1 and 2 of Figure 8B show that the photolabeled MRP1 band decreased in size after treatment with PNGase F. Trypsin digestion of MRP1 shows that N1 and N2 were photolabeled by IAALTC$_4$ (lane 3). After the digested sample was deglycosylated, a 28 kDa fragment labeled with IAALTC$_4$ was generated. This band corresponds to the deglycosylated N2 fragment (lane 4). This demonstrates that MRPr1 can immunoprecipitate the photolabeled MSD0. To confirm this result, we used the same approach on MRP1 variants 4 and 163 (Figure 8C,D). Both of these mutants have an HA epitope in MSD0 that would allow us to immunoprecipitate N2. The deglycosylated 28 kDa or N2 fragment was clearly photolabeled in MRP1 variants 4 and 163. In contrast, the native and deglycosylated N2 fragments were not detected in MRP1 variant 271 (Figure 8E).

DISCUSSION

MRP1 has been shown to interact with and mediate the transport of unconjugated anticancer drugs in addition to normal cell metabolites. Previously, we have mapped the binding domains of several unconjugated substrates that are transported by MRP1 (*22*, *23*). In this study, it was of interest to determine the binding sites of LTC$_4$ in MRP1. For this, a photoreactive analogue of LTC$_4$ was synthesized (IAALTC$_4$) and shown to specifically photoaffinity label MRP1. IAALTC$_4$ binding to MRP1 was saturable and was inhibited by a molar excess of endogenous (LTC$_4$ and GSH) and exogenous (MK571, vincristine, and verapamil) substrates. Together, these results show that IAALTC$_4$ binds to physiologically relevant sites in MRP1.

The increase in photolabeling observed in the presence of 100 μM GSSG was unexpected. Furthermore, we were unable to find any previous report that examined the effect of GSSG on LTC$_4$ binding. Although this increase in photolabeling is not entirely clear, it is possible that the cellular GSH/GSSG ratio influences the interaction between MRP1 and LTC$_4$. In such a system, GSH reduces the affinity of LTC$_4$ for MRP1 while GSSG increases affinity. Thereby, the redox state of a cell would affect the physiological release of LTC$_4$. Interestingly, none of the MRP1 substrates completely inhibit IAALTC$_4$ labeling. To help to understand this, we determined several kinetic parameters pertaining to MRP1−IAALTC$_4$ interactions. The K_m value of 0.42 μM obtained for IAALTC$_4$ shows that it interacts with a high affinity relative to many MRP1 substrates. This K_m value is within the high-affinity range that we (0.17 μM) and others (approximately 0.10 μM) have measured for [^{3}H]LTC$_4$ (*13*). Taken together, it would appear as if MRP1 substrates are not able to completely inhibit IAALTC$_4$ photolabeling due to the high affinity it shares with its parent compound LTC$_4$. This is further illustrated by the observation that the most effective inhibitors of photolabeling, LTC$_4$ and MK571, are higher affinity substrates than the other compounds (GSH, GSSG, verapamil, and vincristine) (*46*−*49*).

The present study demonstrates for the first time that a photoreactive analogue of LTC$_4$ photolabels MSD0 and TM

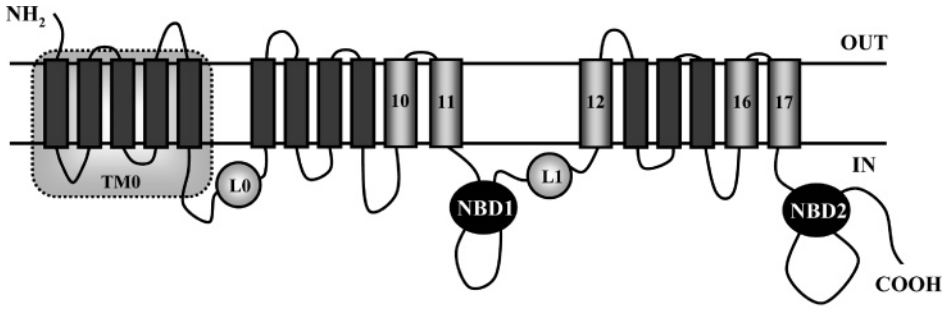

Summary of the photolabelling intensity in various regions of MRP1 by different photoreactive compounds

Compound	*TMD0*	*L0*	*TM 10-11*	*L1*	*TM 12*	*TM 16-17*
IACI	-	-	+	-	-	++
IAARh123	-	-	+	-	-	+++
IAAGSH	-	+	++	+	-	+++
$IAALTC_4$	+	-	+	-	+	++++

FIGURE 9: Topological illustration of photolabeling sites in MRP1 for several compounds. The above diagram illustrates the predicted topological organization of the transmembrane segments in MRP1. The regions that have been found to interact with photoreactive compounds are shaded in gray: TMD0, L0, TM 10, TM 11, L1, TM 12, TM 16, and TM 17.

12 of MRP1, in addition to sequences in TM 10−11 and TM 16−17. Previously, we have reported the significance of TM 10−11 and TM 16−17 with several photoreactive compounds: IACI, IAARh123, and IAAGSH (*22*, *23*). Using two different photoreactive drugs [[^{125}I]LY475776 and an analogue of agosterol A (AG-A)], it was also shown that sequences within TM 16−17 are photoaffinity labeled (*53*). Furthermore, specific amino acid substitutions within TM 10−11 and TM 16−17 have been shown to alter drug binding and transport (*24*−*27*). Together, these findings point to the importance of these two regions in forming a substrate binding site.

In addition to the above-mentioned TM helices, we demonstrate that $IAALTC_4$ photolabeled a polypeptide encompassing TM 12 and a portion of the extracellular loop between TM 12 and TM 13. Interestingly, a previous photolabeling study using murine *mdr*1b P-glycoprotein identified a similar binding site (*54*). In that study, a 7-*p*-benzoyldihydrocinnamol (7-BzDC) analogue of Taxol was used. 7-BzDC−Taxol photolabels a region encompassed by TM 7 and half of TM 8 plus the intervening extracellular loop of *mdr*1b. This region of *mdr*1b is topologically equivalent to TM 12 of MRP1. In addition, mutations in TM 7 of P-gp1 have been found to decrease drug resistance (*55*, *56*). These similarities are not surprising considering that other topologically equivalent regions in ABC transporters are important for substrate recognition (as indicated above). Given this, the present report is the first to implicate this region in the MRP1 drug binding site.

The results presented in this study indicate that a region within the boundary of the N2 peptide directly interacts with $IAALTC_4$. Both MSD0 and an NH_2-terminal portion of L0 are found within the N2 peptide. Efficient photolabeling of MRP1 by [^{3}H]LTC_4 is dependent on part of the L0 region between Cys^{208} and Asn^{260} (*57*) but not MSD0 (*58*). Interestingly, L0 itself is not photolabeled by [^{3}H]LTC_4 (*58*). Furthermore, a portion of L0 between amino acids 204−280 is important for [^{3}H]LTC_4 transport. Given this, the precise function of L0 is still not completely defined. Similarly, the role of MSD0 in substrate binding or transport remains unclear. Earlier studies have shown LTC_4 transport to drastically decrease when MSD0 or TM1 is removed (*9*). Other studies show that MRP1-mediated transport of LTC_4 was reduced when portions of MSD0 are exchanged with equivalent regions of MRP2 (or ABCC2) (*9*, *58*). Furthermore, two studies found that mutating specific Cys residues within MSD0 dramatically reduces LTC_4 transport (*29*, *32*). Therefore, much of the work to date indicates that at least some portion of MSD0 is critical for MRP1-mediated transport. Conversely, it was found that LTC_4 transport is unaffected in a truncated MRP1 mutant lacking MSD0 (*59*). In the current study we showed that the N2 fragment is photolabeled with $IAALTC_4$ (Figure 5A,B). These findings are supported by the deglycosylation of N2 whereby the native and deglycosylated N2 fragments were photolabeled by $IAALTC_4$. The MRPr1 mAb was used to isolate the deglycosylated and photolabeled N2 fragment (Figure 8B). Furthermore, the same $IAALTC_4$-labeled fragment was purified from MRP1 variants 4 and 163 using the anti-HA mAb (Figure 8C,D). Taken together, our results show that MSD0 was able to bind LTC_4. A previous study found that [^{3}H]LTC_4 does not photolabel MSD0 (*36*). This study also showed that photolabeling of the COOH-proximal half of MRP1 with [^{3}H]LTC_4 is limited to TM 14−17, thereby excluding TM 12. These discrepancies may stem from our different experimental systems. While this report used HA variants of MRP1 for $IAALTC_4$ photolabeling, the previous study photolabeled coexpressed truncated fragments of MRP1; neither study used unmodified full-length MRP1. Alternatively, the addition of the photoreactive moiety onto LTC_4 (i.e., $IAALTC_4$) could extend beyond the immediate region of LTC_4 binding domain(s) and photolabel a nearby domain such as TM 12. [^{3}H]LTC_4 is a useful compound because it is functionally and structurally identical to native LTC_4. Conversely, its UV cross-linking efficiency is different from our rapid photoreactive analogue. It is conceivable that photolabeling with [^{3}H]LTC_4 would not allow for the detection of weakly photolabeled sequences, whereas $IAALTC_4$ has a high specific activity which allowed us to see photolabeling of the N2 fragment. Taken together,

although the results of this study show for the first time a direct binding of $IAALTC_4$ to sequences in MRP1 that encode MSD0, higher resolution drug binding studies are required to better define the sequences of MSD0 that directly mediate LTC_4 binding.

To understand the relevance of the regions photolabeled by $IAALTC_4$, we examined the structures of ABC transporters that are currently available. Two high-resolution structures of ABC proteins have been solved. These are the lipid A transporters, MsbA, from *Escherichia coli* (EC-MsbA) and from *Vibrio cholera* (VC-MsbA) (*60*, *61*). Each transporter is a dimer composed of two subunits, each containing six transmembrane passes. The shape of the EC-MsbA dimer resembles an upside down V. The arms of this structure are separated by 40 Å on the cytoplasmic side of the plasma membrane. The VC-MsbA structure is similar although the arms are closer together. A recent study used these structures to model the MRP1 substrate binding site(s) (*25*). This work proposes that specific amino acids in TM 10−11 and TM 16−17 make up an "aromatic basket" for substrate binding and are located at the edges of the V-like gap. We have also identified these same transmembrane domains as essential for substrate binding. As indicated in the table in Figure 9, all of the photoreactive drugs that we have previously examined interact directly with TM 10−11 and TM 16−17, including $IAALTC_4$.

Interestingly, the MsbA structures predict that TM 1 in each subunit is located adjacent to TM 5 and TM 6 (*60*, *61*). This information sheds light on our finding that TM 12 was photolabeled by $IAALTC_4$. The MsbA TM 1 and TM 5−6 are topologically equivalent to TM 12 and TM 16−17. Therefore, TM 12 may be photolabeled because of its proximity to the TM 16−17 binding region. TM 12 may also contribute amino acids that directly interact with LTC_4. In either case, this study demonstrates how photolabeling studies in conjunction with the newly resolved ABC protein structures will surely improve the understanding of all drug binding studies.

In summary, our findings revealed several interesting attributes of LTC_4 binding with MRP1. (i) Its binding sites were found within TM 10−11 and TM 16−17, which are topologically equivalent to TM 5−6 and TM 11−12 in P-gp1. (ii) The photolabeling of TM 12 confirms structural data from other ABC transporters and places this TM helix within close proximity to TM 16−17. TM 12 may also make up part of the multidrug binding site. Finally, (iii) $IAALTC_4$ interacted with and photolabeled the MSD0 domain of MRP1. This observation was confirmed using several mAbs to specifically isolate the N2 fragment in both its native and deglycosylated form. These results demonstrate two important characteristics of MRP1. First, the interaction of LTC_4 with TM 10−11 and TM 16−17 furthers the possibility that ABC transporters share structural motifs to make up a multidrug binding site. Second, the interactions between LTC_4 and TMD0 indicate that MRP1 may contain separate regions necessary for binding its endogenous substrate.

ACKNOWLEDGMENT

We thank Nicholas Patocka for assistance with preparation of Figure 5.

REFERENCES

1. Riordan, J. R., and Ling, V. (1979) Purification of P-glycoprotein from plasma membrane vesicles of Chinese hamster ovary cell mutants with reduced colchicine permeability, *J. Biol. Chem. 254*, 12701−12705.
2. Scala, S., Akhmed, N., Rao, U. S., Paull, K., Lan, L. B., Dickstein, B., Lee, J. S., Elgemeie, G. H., Stein, W. D., and Bates, S. E. (1997) P-glycoprotein substrates and antagonists cluster into two distinct groups, *Mol. Pharmacol. 51*, 1024−1033.
3. Gottesman, M. M., and Pastan, I. (1993) Biochemistry of multidrug resistance mediated by the multidrug transporter, *Annu. Rev. Biochem. 62*, 385−427.
4. Mirski, S. E., Gerlach, J. H., and Cole, S. P. (1987) Multidrug resistance in a human small cell lung cancer cell line selected in adriamycin, *Cancer Res. 47*, 2594−2598.
5. Cole, S. P. (1990) Patterns of cross-resistance in a multidrug-resistant small-cell lung carcinoma cell line, *Cancer Chemother. Pharmacol. 26*, 250−256.
6. Cole, S. P. C., Bhardwaj, G., Gerlach, J. H., Mackie, C. E., Almquist, K. C., Stewart, A. J., Kurz, E. U., Duncan, A. M. V., and Deeley, R. G. (1992) Overexpression of a transport gene in a multidrug-resistant human lung cancer cell line, *Science 258*, 1650−1654.
7. Borst, P., and Schinkel, A. H. (1997) Genetic dissection of the function of mammalian P-glycoproteins, *Trends Genet. 13*, 217−222.
8. Germann, U. A. (1996) P-glycoprotein—A mediator of multidrug resistance in tumour cells, *Eur. J. Cancer 32A*, 927−944.
9. Gao, M., Yamazaki, M., Loe, D. W., Westlake, C. J., Grant, C. E., Cole, S. P. C., and Deeley, R. G. (1998) Multidrug resistance protein, identification of the regions required for active transport of leukotriene C_4, *J. Biol. Chem. 273*, 10733−10740.
10. Hooijberg, J. H., Broxterman, H. J., Kool, M., Assaraf, Y. G., Peters, G. J., Noordhuis, P., Scheper, R. J., Borst, P., Pinedo, H. M., and Jansen, G. (1999) Antifolate resistance mediated by the multidrug resistance proteins MRP1 and MRP2, *Cancer Res. 59*, 2532−2535.
11. Cole, S. P. C., Sparks, K. E., Fraser, K., Loe, D. W., Grant, C. E., Wilson, G. M., and Deeley, R. G. (1994) Pharmacological characterization of multidrug resistance MRP-transfected human tumor cells, *Cancer Res. 54*, 5902−5910.
12. Holland, I. B. (2003) *ABC proteins: from bacteria to man*, Academic Press, London and San Diego.
13. Loe, D. W., Almquist, K. C., Deeley, R. G., and Cole, S. P. (1996) Multidrug resistance protein (MRP)-mediated transport of leukotriene C4 and chemotherapeutic agents in membrane vesicles. Demonstration of glutathione-dependent vincristine transport, *J. Biol. Chem. 271*, 9675−9682.
14. Loe, D. W., Stewart, R. K., Massey, T. E., Deeley, R. G., and Cole, S. P. (1997) ATP-dependent transport of aflatoxin B1 and its glutathione conjugates by the product of the multidrug resistance protein (MRP) gene, *Mol. Pharmacol. 51*, 1034−1041.
15. Drazen, J. M., Israel, E., and O'Byrne, P. M. (1999) Treatment of asthma with drugs modifying the leukotriene pathway, *N. Engl. J. Med. 340*, 197−206.
16. Samuelsson, B., Dahlen, S. E., Lindgren, J. A., Rouzer, C. A., and Serhan, C. N. (1987) Leukotrienes and lipoxins: structures, biosynthesis, and biological effects, *Science 237*, 1171−1176.
17. Wijnholds, J., Evers, R., van Leusden, M. R., Mol, C. A., Zaman, G. J., Mayer, U., Beijnen, J. H., van der Valk, M., Krimpenfort, P., and Borst, P. (1997) Increased sensitivity to anticancer drugs and decreased inflammatory response in mice lacking the multidrug resistance-associated protein, *Nat. Med. 3*, 1275−1279.
18. Robbiani, D. F., Finch, R. A., Jager, D., Muller, W. A., Sartorelli, A. C., and Randolph, G. J. (2000) The leukotriene C(4) transporter MRP1 regulates CCL19 (MIP-3beta, ELC)-dependent mobilization of dendritic cells to lymph nodes, *Cell 103*, 757−768.
19. Cole, S. P., and Deeley, R. G. (1998) Multidrug resistance mediated by the ATP-binding cassette transporter protein MRP, *BioEssays 20*, 931−940.
20. Bakos, E., Hegedus, T., Hollo, Z., Welker, E., Tusnady, G. E., Zaman, G. J., Flens, M. J., Varadi, A., and Sarkadi, B. (1996) Membrane topology and glycosylation of the human multidrug resistance-associated protein, *J. Biol. Chem. 271*, 12322−12326.
21. Hipfner, D. R., Almquist, K. C., Leslie, E. M., Gerlach, J. H., Grant, C. E., Deeley, R. G., and Cole, S. P. (1997) Membrane topology of the multidrug resistance protein (MRP). A study of

glycosylation-site mutants reveals an extracytosolic NH2 terminus, *J. Biol. Chem. 272*, 23623−23630.
22. Daoud, R., Julien, M., Gros, P., and Georges, E. (2001) Major photoaffinity drug binding sites in multidrug resistance protein 1 (MRP1) are within transmembrane domains 10−11 and 16−17, *J. Biol. Chem. 276*, 12324−12330.
23. Karwatsky, J., Daoud, R., Cai, J., Gros, P., and Georges, E. (2003) Binding of a photoaffinity analogue of glutathione to MRP1 (ABCC1) within two cytoplasmic regions (L0 and L1) as well as transmembrane domains 10−11 and 16−17, *Biochemistry 42*, 3286−3294.
24. Ito, K., Oleschuk, C. J., Westlake, C., Vasa, M. Z., Deeley, R. G., and Cole, S. P. (2001) Mutation of Trp1254 in the multispecific organic anion transporter, multidrug resistance protein 2 (MRP2) (ABCC2), alters substrate specificity and results in loss of methotrexate transport activity, *J. Biol. Chem. 276*, 38108−38114.
25. Campbell, J. D., Koike, K., Moreau, C., Sansom, M. S., Deeley, R. G., and Cole, S. P. (2004) Molecular modeling correctly predicts the functional importance of Phe594 in transmembrane helix 11 of the multidrug resistance protein, MRP1 (ABCC1), *J. Biol. Chem. 279*, 463−468.
26. Koike, K., Oleschuk, C. J., Haimeur, A., Olsen, S. L., Deeley, R. G., and Cole, S. P. (2002) Multiple membrane-associated tryptophan residues contribute to the transport activity and substrate specificity of the human multidrug resistance protein, MRP1, *J. Biol. Chem. 277*, 49495−49503.
27. Zhang, D. W., Cole, S. P., and Deeley, R. G. (2002) Determinants of the substrate specificity of multidrug resistance protein 1: role of amino acid residues with hydrogen bonding potential in predicted transmembrane helix 17, *J. Biol. Chem. 277*, 20934−20941.
28. Zhang, D. W., Cole, S. P., and Deeley, R. G. (2001) Identification of a nonconserved amino acid residue in multidrug resistance protein 1 important for determining substrate specificity: evidence for functional interaction between transmembrane helices 14 and 17, *J. Biol. Chem. 276*, 34966−34974.
29. Leslie, E. M., Letourneau, I. J., Deeley, R. G., and Cole, S. P. (2003) Functional and structural consequences of cysteine substitutions in the NH2 proximal region of the human multidrug resistance protein 1 (MRP1/ABCC1), *Biochemistry 42*, 5214−5224.
30. Ito, K., Olsen, S. L., Qiu, W., Deeley, R. G., and Cole, S. P. (2001) Mutation of a single conserved tryptophan in multidrug resistance protein 1 (MRP1/ABCC1) results in loss of drug resistance and selective loss of organic anion transport, *J. Biol. Chem. 276*, 15616−15624.
31. Haimeur, A., Deeley, R. G., and Cole, S. P. (2002) Charged amino acids in the sixth transmembrane helix of multidrug resistance protein 1 (MRP1/ABCC1) are critical determinants of transport activity, *J. Biol. Chem. 277*, 41326−41333.
32. Yang, Y., Chen, Q., and Zhang, J. T. (2002) Structural and functional consequences of mutating cysteine residues in the amino terminus of human multidrug resistance-associated protein 1, *J. Biol. Chem. 277*, 44268−44277.
33. Leier, I., Jedlitschky, G., Buchholz, U., Cole, S. P., Deeley, R. G., and Keppler, D. (1994) The MRP gene encodes an ATP-dependent export pump for leukotriene C4 and structurally related conjugates, *J. Biol. Chem. 269*, 27807−27810.
34. Leier, I., Jedlitschky, G., Buchholz, U., and Keppler, D. (1994) Characterization of the ATP-dependent leukotriene C4 export carrier in mastocytoma cells, *Eur. J. Biochem. 220*, 599−606.
35. Loe, D. W., Almquist, K. C., Cole, S. P., and Deeley, R. G. (1996) ATP-dependent 17 beta-estradiol 17-(beta-D-glucuronide) transport by multidrug resistance protein (MRP). Inhibition by cholestatic steroids, *J. Biol. Chem. 271*, 9683−9689.
36. Qian, Y. M., Qiu, W., Gao, M., Westlake, C. J., Cole, S. P., and Deeley, R. G. (2001) Characterization of binding of leukotriene C4 by human multidrug resistance protein 1: evidence of differential interactions with NH2- and COOH-proximal halves of the protein, *J. Biol. Chem. 276*, 38636−38644.
37. Kast, C., and Gros, P. (1997) Topology mapping of the amino-terminal half of multidrug resistance-associated protein by epitope insertion and immunofluorescence, *J. Biol. Chem. 272*, 26479−26487.
38. Kast, C., and Gros, P. (1998) Epitope insertion favors a six transmembrane domain model for the carboxy-terminal portion of the multidrug resistance-associated protein, *Biochemistry 37*, 2305−2313.
39. Lowry, O. H., Rosebrough, N. J., Farr, A. L., and Randall, R. J. (1951) Protein measurement with the Folin phenol reagent, *J. Biol. Chem. 193*, 265−275.
40. Nare, B., Prichard, R. K., and Georges, E. (1994) Characterization of rhodamine 123 binding to P-glycoprotein in human multidrug-resistant cells, *Mol. Pharmacol. 45*, 1145−1152.
41. Georges, E., Zhang, J. T., and Ling, V. (1991) Modulation of ATP and drug binding by monoclonal antibodies against P-glycoprotein, *J. Cell Physiol. 148*, 479−484.
42. Fairbanks, G., Steck, T. L., and Wallach, D. F. (1971) Electrophoretic analysis of the major polypeptides of the human erythrocyte membrane, *Biochemistry 10*, 2606−2617.
43. Coligan, J. E. (2001) *Current protocols in protein science*, Wiley, New York.
44. Towbin, H., Staehelin, T., and Gordon, J. (1979) Electrophoretic transfer of proteins from polyacrylamide gels to nitrocellulose sheets: procedure and some applications, *Proc. Natl. Acad. Sci. U.S.A. 76*, 4350−4354.
45. Leier, I., Jedlitschky, G., Buchholz, U., Center, M., Cole, S. P., Deeley, R. G., and Keppler, D. (1996) ATP-dependent glutathione disulphide transport mediated by the MRP gene-encoded conjugate export pump, *Biochem. J. 314* (Part 2), 433−437.
46. Jedlitschky, G., Leier, I., Buchholz, U., Center, M., and Keppler, D. (1994) ATP-dependent transport of glutathione S-conjugates by the multidrug resistance-associated protein, *Cancer Res. 54*, 4833−4836.
47. Loe, D. W., Deeley, R. G., and Cole, S. P. (1998) Characterization of vincristine transport by the M(r) 190,000 multidrug resistance protein (MRP): evidence for cotransport with reduced glutathione, *Cancer Res. 58*, 5130−5136.
48. Rappa, G., Lorico, A., Flavell, R. A., and Sartorelli, A. C. (1997) Evidence that the multidrug resistance protein (MRP) functions as a co-transporter of glutathione and natural product toxins, *Cancer Res. 57*, 5232−5237.
49. Gekeler, V., Ise, W., Sanders, K. H., Ulrich, W. R., and Beck, J. (1995) The leukotriene LTD4 receptor antagonist MK571 specifically modulates MRP associated multidrug resistance, *Biochem. Biophys. Res. Commun. 208*, 345−352.
50. Jedlitschky, G., Leier, I., Buchholz, U., Barnouin, K., Kurz, G., and Keppler, D. (1996) Transport of glutathione, glucuronate, and sulfate conjugates by the MRP gene-encoded conjugate export pump, *Cancer Res. 56*, 988−994.
51. Hipfner, D. R., Gao, M., Scheffer, G., Scheper, R. J., Deeley, R. G., and Cole, S. P. (1998) Epitope mapping of monoclonal antibodies specific for the 190-kDa multidrug resistance protein (MRP), *Br. J. Cancer 78*, 1134−1140.
52. Hipfner, D. R., Almquist, K. C., Stride, B. D., Deeley, R. G., and Cole, S. P. (1996) Location of a protease-hypersensitive region in the multidrug resistance protein (MRP) by mapping of the epitope of MRP-specific monoclonal antibody QCRL-1, *Cancer Res. 56*, 3307−3314.
53. Mao, Q., Qiu, W., Weigl, K. E., Lander, P. A., Tabas, L. B., Shepard, R. L., Dantzig, A. H., Deeley, R. G., and Cole, S. P. (2002) GSH-dependent photolabeling of multidrug resistance protein MRP1 (ABCC1) by [^{125}I]LY475776. Evidence of a major binding site in the COOH-proximal membrane spanning domain, *J. Biol. Chem. 277*, 28690−28699.
54. Wu, Q., Bounaud, P. Y., Kuduk, S. D., Yang, C. P., Ojima, I., Horwitz, S. B., and Orr, G. A. (1998) Identification of the domains of photoincorporation of the 3′- and 7-benzophenone analogues of taxol in the carboxyl-terminal half of murine mdr1b P-glycoprotein, *Biochemistry 37*, 11272−11279.
55. Loo, T. W., and Clarke, D. M. (1996) Mutational analysis of the predicted first transmembrane segment of each homologous half of human P-glycoprotein suggests that they are symmetrically arranged in the membrane, *J. Biol. Chem. 271*, 15414−15419.
56. Loo, T. W., and Clarke, D. M. (1993) Functional consequences of proline mutations in the predicted transmembrane domain of P-glycoprotein, *J. Biol. Chem. 268*, 3143−3149.
57. Westlake, C. J., Qian, Y. M., Gao, M., Vasa, M., Cole, S. P., and Deeley, R. G. (2003) Identification of the structural and functional boundaries of the multidrug resistance protein 1 cytoplasmic loop 3, *Biochemistry 42*, 14099−14113.
58. Konno, T., Ebihara, T., Hisaeda, K., Uchiumi, T., Nakamura, T., Shirakusa, T., Kuwano, M., and Wada, M. (2003) Identification

of domains participating in the substrate specificity and subcellular localization of the multidrug resistance proteins MRP1 and MRP2, *J. Biol. Chem. 278*, 22908−22917.

59. Bakos, E., Evers, R., Szakacs, G., Tusnady, G. E., Welker, E., Szabo, K., de Haas, M., van Deemter, L., Borst, P., Varadi, A., and Sarkadi, B. (1998) Functional multidrug resistance protein (MRP1) lacking the N-terminal transmembrane domain, *J. Biol. Chem. 273*, 32167−32175.
60. Chang, G., and Roth, C. B. (2001) Structure of MsbA from *E. coli*: a homolog of the multidrug resistance ATP binding cassette (ABC) transporters, *Science 293*, 1793−1800.
61. Chang, G. (2003) Structure of MsbA from *Vibrio cholera*: a multidrug resistance ABC transporter homolog in a closed conformation, *J. Mol. Biol. 330*, 419−430.

BI048853H